Asymmetric lamb wave propagation and mode isolation in thin plate with spatiotemporal periodic stiffness

Zhao, Liuxian; Lai, Chang Quan

2019

Zhao, L. & Lai, C. Q. (2019). Asymmetric lamb wave propagation and mode isolation in thin plate with spatiotemporal periodic stiffness. Journal of Vibration and Acoustics, 141(5), 051005-. https://dx.doi.org/10.1115/1.4043509

https://hdl.handle.net/10356/105470

https://doi.org/10.1115/1.4043509

Published in *J. Vib. Acoust.* **141**, 051005-051005–6 (2019). DOI: 10.1115/1.4043509

Asymmetric Lamb wave propagation and mode isolation in thin plate with spatiotemporal periodic stiffness

Liuxian Zhao, Chang Quan Lai*

Temasek Laboratories, Nanyang Technological University, 50 Nanyang Drive, Singapore 637553
***E-mail: cqlai@ntu.edu.sg

Abstract

The Lamb wave propagation through a thin plate with periodic spatiotemporal variation of material property was investigated through numerical simulations. It was found that regular oscillations of the Young's modulus in both space and time can lead to the creation of distinct band gaps for different modes of Lamb wave. Moreover, the dispersion relation for each mode was dependent on the direction of wave propagation (*i.e.* non-reciprocal). These results allow the Lamb wave modes to be reduced to a single mode travelling in a single direction for specific frequencies. This frequency range was observed to widen with increasing modulation amplitude of the Young's modulus but was not significantly altered by the modulation frequency. The insights derived from this study indicate that spatiotemporal control of material property can be used to effectively isolate Lamb wave modes and reduce reflections, leading to an improvement in the accuracy of the structural health monitoring of materials.

Keywords: Directional wave propagation, Lamb wave, Spatiotemporal modulation, Non-reciprocal effect

1. Introduction

Lamb wave is an elastic wave that propagates through thin solid structures with free boundary conditions at the top and bottom surfaces. Its unique characteristic is that it can propagate for long distances without significant attenuation, which is instrumental to the non-destructive defect monitoring of large structures [1-5].

Despite the low transmission loss, however, Lamb wave continues to pose complications in the structural health monitoring (SHM) technique, mainly because it is composed of many propagation modes, possesses dispersive characteristics and the wave signals on the receiving end tend to be mixed with reflected and converted wave modes, making intepretation extremely challenging.

To circumvent these difficulties, filters and wave guides had previously been developed to isolate specific modes of the Lamb wave [6, 7], as well as to confine the wave propagation to specific directions [8]. The strategies for mode isolation revolve mainly around the use of phononic crystals, which prevents the transmission of selective wave frequencies through the action of Bragg scattering [9-21]. To achieve unidirectional transmission, on the other hand, requires breaking either the spatial inversion symmetry or the time-reversal symmetry [22]. For instance, Chen *et. al.* [23] investigated asymmetric Lamb wave propagation by introducing metallic gratings with graded depth,

which altered the threshold frequency of the fundamental antisymmetric Lamb mode and the fundamental symmetric Lamb mode at different locations of the graded gratings. Li *et. al.* [24] also studied the asymmetric Lamb wave transmission through the use of a simple linear acoustic system, which consisted of periodic gratings on both sides of a thin plate immersed in fluid. The gratings on each side were misaligned with respect to each other in order to disrupt the spatial symmetry of the structure and facilitate the asymmetric transmission of Lamb wave. The frequency range at which this occurs can be controlled by adjusting the dimensions of the double layer metallic plate. Furthermore, directional edge wave propagation that is topologically protected from back-scattering can also be achieved using topological acoustic metamaterials, which were designed by breaking space-inversion symmetry to achieve acoustic pseudo-spins and pseudo-spin-dependent effective fields [25, 26].

Another method of inducing directional wave propagation would be to vary the physical properties of the medium over time and space. Croenne *et. al.* [27] had shown that the breakdown of time-reversal symmetry can be achieved through spatiotemporal modulation of the physical characteristics of a one-dimensional phononic crystal. This was realized through the use of stacked piezoelectric elements which were excited in a sequential manner. At certain excitation velocities, directional wave propagation was observed in this system. In a similar study, Swinteck *et. al.* [28] also demonstrated that bulk elastic waves propagating in a time-dependent superlattice can achieve unidirectional wave propagation that removes reflected waves. In addition, Trainiti *et. al.* [29] described the dispersion diagrams of elastic waves propagating in beams with material properties that were periodic over time and space. They studied both non-dispersive longitudinal motion and dispersive transverse motion in the low-frequency range using the Euler–Bernoulli beam theory. The dispersion diagrams demonstrated a new class of band gaps that allow wave propagation in one direction only, and were therefore referred to as non-reciprocal or directional band gaps. Such non-reciprocal wave propagation has also been studied through spatiotemporal modulation of the physical properties of phononic crystals and metamaterials [30-35].

Zanjani *et. al.* [36] presented one-way conversion between symmetric and antisymmetric shear horizontal modes of an unbounded plate using time-space periodic material properties, which showed that the spatio-temporally modulation of material property can break the symmetry of mode conversion in forward and backward directions. Wang *et. al.* [37] experimentally observed non-reciprocal wave propagation in a spatiotemporally modulated phononic chain for sound waves, which was the first experimental demonstration of non-reciprocity in a one-dimensional phononic chain. The spatiotemporal modulation was controlled by electro-magnets in a discrete chain of magnetic masses connected by weakly nonlinear springs. This biased modulation breaks time-reversal symmetry and opened a bandgap in the dispersion relation, which showed non-reciprocal sound propagation.

In summary, to date, unidirectional propagation of Lamb wave has been achieved by introducing spatial asymmetry in the material design [24], while unidirectional propagation of bulk elastic wave has been demonstrated through the spatiotemporal modulation of material properties [29]. However, the effect of spatiotemporal modulation on the propagation of Lamb wave remains unclear. Therefore, we attempt to clarify this through numerical simulations in the present study, by periodically varying the Young's modulus of a thin plate in space and time using piezoelectric elements, and studying the resultant propagation of Lamb wave in such a material. The novelty of this work is in the usage of spatiotemporal variation of material property to reduce Lamb wave modes to a single mode that can only travel in a single direction at specific frequencies. This mode isolation and directional propagation is expected to improve the accuracy of applications such as structural health monitoring.

2. Quantitative Modelling

Consider a thin plate with mass density, ρ, Poisson's ratio ν and Young's modulus, E, which is periodically varied along the length of the plate in the x-direction and time domain, t, such that

$$E(x,t) = E_0 + E_m \cos(\omega_m t - k_m x) \qquad (1)$$

Here, we define the modulation wave number, k_m as $2\pi/\lambda_m$ and the modulation angular frequency, ω_m, as $2\pi/T_m$, where λ_m refers to the spatial periodicity and T_m is the temporal periodicity. E_0 refers the native Young's modulus of the plate material while E_m is the

amplitude of modulation. The mass density, $\rho(x, t)$, and Possion's ratio, $\nu(x, t)$, are held constant as ρ_0 and ν_0 respectively. Since aluminum is a material commonly involved in structural health monitoring (SHM) [38], its physical properties are adopted for the thin plate in the current investigation *i.e.* $\rho_0 = 2700$ kg/m^3, $\nu_0 = 0.33$ and $E_0 = 70$ GPa.

For $E_m = 0$, the material stiffness is not modulated and the plate is uniform, and will be referred to as "Constant Plate" in the following. If $E_m \neq 0$, $k_m \neq 0$ and $\omega_m = 0$, then the Young's modulus is periodically varied along the spatial *x* domain only. This will be referred to as the "Spatial Variation Plate". Lastly, if $E_m \neq 0$, $k_m \neq 0$ and $\omega_m \neq 0$, the value of the Young's modulus *E* is periodically modulated along both the spatial *x* domain and temporal *t* domain (equation (1)). We refer to this as the "Spatiotemporal Variation Plate". To simplify this study, we have made the assumption that the shear modulus is varying synchronously with the oscillations of *E* to keep ν constant.

An example of harmonic modulation of Young's modulus *E* is given in Figure 1 based on equation (1), where $E_m = 28$ GPa and $k_m = 20\pi$ m^{-1}. The spatial-only modulation is shown in Figure 1(a) and corresponds to the case with $\omega_m = 0$ rad/s, while spatiotemporal modulation with $\omega_m = 5000\pi$ rad/s is shown in Figure 1 (b). In an otherwise symmetric system, this spatiotemporal modulation introduces the only asymmetry necessary for directional wave propagation.

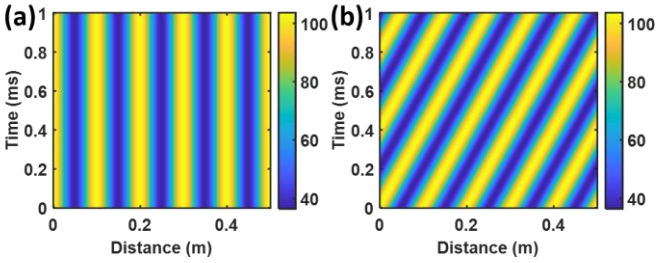

Figure 1: Periodic modulation of Young's modulus in both the space and time domains given by equation (1), (a) spatial-only modulation ($\omega_m = 0$ rad/s), (b) spatiotemporal modulation ($\omega_m = 5000\pi$ rad/s). The color scale bar represents the Young's modulus in GPa.

Next, we present the governing equations of wave propagation in the thin plate with material properties that vary in both space and time domains. In an inhomogeneous linear elastic structure without body force, the equation of motion for displacement vector $u(x, z, t)$ can be written as

$$\rho(x,t)\ddot{u}_i(x,z,t) = \partial_j\left[c_{ijmn}(x,t)\partial_n u_m(x,z,t)\right] \ (i = 1,3) \quad (2)$$

Note that the elastic stiffness c_{ijmn} of the plate is a function of Young's modulus, *E*, and Possion's ratio, *v*, where $c_{11} = \frac{1-\nu}{(1+\nu)(1-2\nu)}E$, $c_{12} = \frac{\nu}{(1+\nu)(1-2\nu)}E$ and $c_{44} = \frac{1}{2(1+\nu)}E$ [39]. If $\rho(x,t)$, $E(x,t)$ and consequently, $c_{ijmn}(x,t)$, are constant in space and time domains, equation (2) will be reduced to the familiar equations of motion for a uniform plate [15]. On the other hand, spatiotemporal modulation of *E* will result in variation of the material stiffness matrix over time and space. It is then possible to express the stiffness matrix by using the Fourier series, so that

$$c_{ijmn}(x,t) = \sum_{p=-\infty}^{+\infty} \hat{c}_p e^{ip(\omega_m t - k_m x)} \quad (3)$$

where $\hat{c}_p$ is the Fourier coefficient of the material properties.

For this study, the thin plate is oriented such that the Lamb wave propagates along the *x* direction, and the plate is bounded by planes *z* = 0 and *z* = *h*, where *h* is the thickness of the plate. This is essentially a two-dimensional problem in *x* and *z* directions, where all field components are independent of the *y* axis. In an inhomogeneous linear elastic medium without body force, based on the Bloch theorem, by expanding the displacement vector $u(x, z, t)$ into the Fourier series, the equation of motion for displacement vector $u(x, z, t)$ can be written as:

$$u(x,z,t) = \sum_{n=-\infty}^{+\infty} \hat{c}_p e^{i(kx-\omega t)} e^{in(\omega_m t - k_m x)} \hat{U}_n e^{ik_z z} \quad (4)$$

The top plane, *z* = *h*, and bottom plane, *z* = 0, of the plate are stress-free, and therefore,

$$T_{n3}\big|_{z=0,h} = c_{i3mn}\big|_{z=0,h} = 0, \ (n = 1, 3) \quad (5)$$

where T_{n3} is the stress components acting in the normal and transverse direction in a plane and *h* is the plate thickness [14]. In the following, numerical simulations using Comsol software is applied to solve the above

equations and calculate the dispersion curves and wave propagations.

3. Numerical Simulations

3.1 Numerical model

In the numerical simulations conducted using ANSYS 15.0 [40], a thin plate with $L \times H = 14 \times 0.05$ m was first constructed using the four nodes structure element PLANE42 (Figure 2). There were absorbing layers (blue blocks in Figure 2) with dimensions, $L_a \times H_a = 2 \times 0.05$ m, at the two ends of the plate in order to minimize the reflected waves [41]. The unit cell length, λ_m, was 0.1 m and the plate was under free boundary conditions.

Excitation of the thin plate was carried out in the middle of the plate ($x = 0$) with a frequency sweep signal in the range of 5 – 45 kHz (Figure 2(b) and Figure 2(c)). This excitation was applied via a piezoelectric transducer (PZT) which converts periodic electrical signals into mechanical oscillations [42]. The dimensions of PZT were $L_{PZT} \times H_{PZT} = 0.2 \times 0.01$ m.

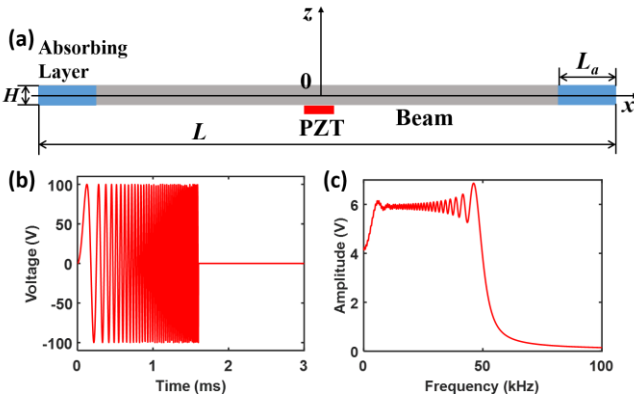

Figure 2: Numerical model for Lamb wave propagation in a thin plate, (a) schematic of a thin plate excited using PZT at the center location, a single PZT is used at the bottom of the plate to generate both symmetric and antisymmetric Lamb wave modes, (b) a wide band frequency sweep signal, and (c) its frequency spectrum using Fourier transform (FFT).

3.2 Dispersion curve analysis

In this study, three different models were investigated: (i) Constant Plate model, where $E_0 = 70$ GPa, $E_m = 0$ GPa, $k_m = 0$ m^{-1} and $\omega_m = 0$ rad/s, (ii) Spatial Variation Plate, where $E_0 = 70$ GPa, $E_m = 42$ GPa, $k_m = 20\pi$ m^{-1} and $\omega_m = 0$ rad/s, and (iii) Spatiotemporal Variation Plate, where $E_0 = 70$ GPa, $E_m = 42$ GPa, $k_m = 20\pi$ m^{-1} and $\omega_m = 5000\pi$ rad/s. The Constant Plate and Spatial Variation Plate act as controls to evaluate the performance of the Spatiotemporal Variation Plate.

The displacement information $u(x, t)$ of the structure was calculated numerically. The results are plotted in the left column of Fig. 3 *i.e.* Figure 3(a), (c) and (e) which show the Lamb wave propagation in time and space domains. The dispersion characteristics of the three models was obtained by performing the two-dimensional Fast Fourier transform (2DFFT) on the displacement fields $u(x, t)$ to compute the frequency-wavenumber data $U(\kappa, \omega)$ [43], *i.e.*

$$U(\kappa,\omega) = \int_{-\infty}^{+\infty}\int_{-\infty}^{+\infty} u(x,t)e^{-i(\omega t-\kappa x)}dxdt \quad (6)$$

The results are presented in the right column of Figure 3 *i.e.* Figure 3(b), (d) and (f). From Figure 3(b), it can be seen that there was no bandgap for Lamb wave propagating through a Constant Plate, which is expected. Both the symmetric (S0) and antisymmetric (A0) modes can pass through the structure for all frequencies.

For the Spatial Variation Plate (Figure 3(d); magnified plot in figure 3(g)), bandgaps were observed for the Lamb wave modes, S0 and A0, at f = 19.17 - 27.33 kHz and f = 20.04 – 22.38 kHz respectively. This suggests that the Lamb wave mode, A0, can be isolated from S0 in the frequencies 19.17 – 20.04 kHz and 22.38 – 27.33 kHz. However, because the bandgaps are symmetric with respect to k, the propagation of A0 would be identical in the $+x$ and $-x$ directions (*i.e.* cannot isolate reflected waves from propagating waves).

For the case of the Spatiotemporal Variation Plate (Figure 3(f); magnified plot in figure 3(h)), however, it can be seen that the bandgap for S0 was f = 18.15 – 25.73 kHz for $k < 0$ and f = 20.77 – 28.36 kHz for $k > 0$. Similarly, the bandgap for A0 was f = 17.42 – 19.75 kHz for $k < 0$ and f = 21.94 – 25 kHz for $k > 0$. These results not only indicate that A0 and S0 can be separated, but the propagating waves can be isolated from the reflected waves as well, because of the asymmetry of the dispersion curves about $k = 0$.

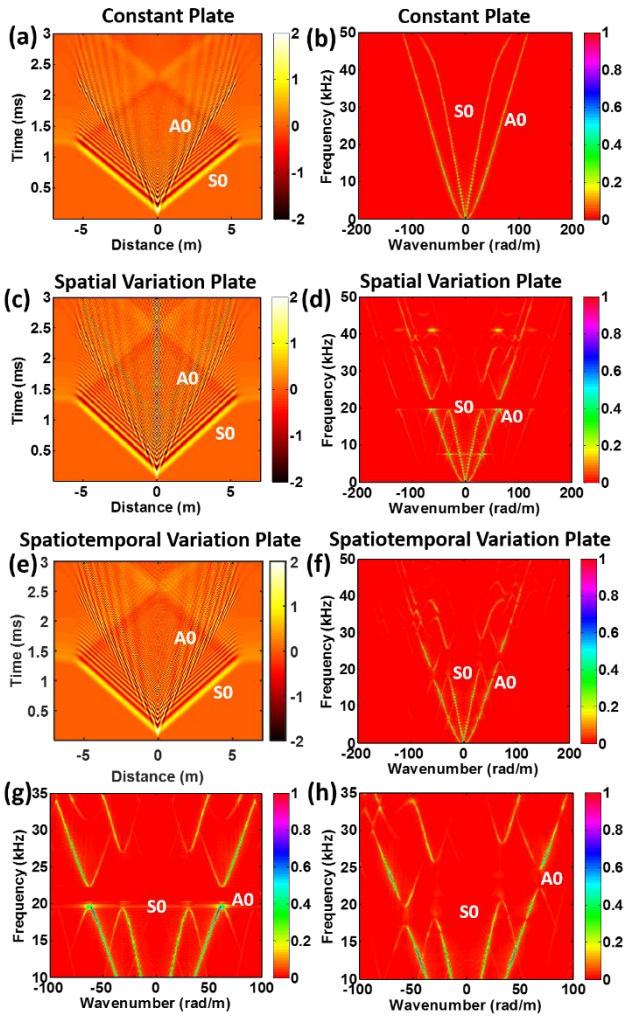

Figure 3: (a) Time-space plot and (b) frequency-wavenumber (f - k) plot for the Constant Plate. (c) Time-space plot and (d) frequency-wavenumber (f - k) plot of the Spatial Variation Plate. (e) Time-space plot and (f) frequency-wavenumber (f - k) plot of the Spatiotemporal Variation Plate. (g) Magnified view of plot in (d). (h) Magnified view of plot in (f). A0 and S0 refer to the asymmetric Lamb mode and symmetric Lamb mode respectively. The color scale bar represents the displacement in the thickness direction (mm).

To ascertain this, a 50-count Hanning-windowed tone burst signal with center frequency f_c = 24 kHz was used to excite the thin plate. Based on the dispersion diagram in Figure 3(h), at this frequency, the only Lamb wave propagation that can take place is A0 in the -x direction. The displacement, u (x, t), was computed numerically and plotted with respect to x and t in Figure 4(a). It is clear that the only observable wave propagation is the A0 mode in the -x direction. The waterfall plot, which tracks the Lamb wave at nine different locations (x = -4, -3, -2, -1, 0, 1, 2, 3, 4 m), is also shown in Figure 4(b) and gives the same result. Spatiotemporal modulation of a thin plate's Young's modulus is therefore an effective method of achieving robust unidirectional wave propagation.

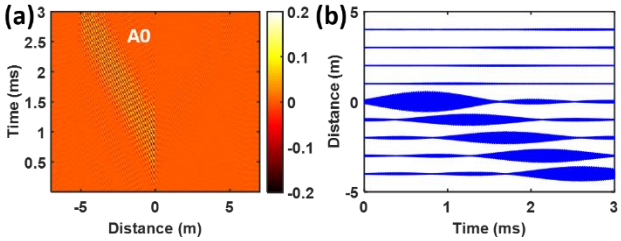

Figure 4: Time-space analysis of the Spatiotemporal Variation Plate using central frequency f = 24 kHz, (a) time-space plot, (b) time-space plot at nine different locations. The color scale bar represents the displacement in the thickness direction (mm).

3.3 Effect of amplitude and frequency of material property modulation

Going further, the influence of modulation parameters on the frequency bands for modal isolation and directional propagation was investigated. In the following parametric studies, we aim to obtain the frequency range of the propagating wave where the A0 mode can propagate unidirectionally in the -x direction but propagation of S0 mode is prohibited in both +x and -x directions.

First, we varied the amplitude of the Young's modulus modulation, E_m = [15 47, 52] GPa, while keeping the angular frequency of modulation, ω_m, constant at 5000π rad/s. The result is given in Figure 5(a), where the red lines represent the frequencies for which isolation *and* directional propagation of A0 mode can take place. It can be observed that increasing E_m leads to an increase in the viable frequency bandwidth and a decrease in average frequency. The increase in bandwidth arises from wider frequency bands for

directional wave propagation with increasing E_m, which is in line with previous results [29].

Next, we varied the angular frequency modulation, $\omega_m = [3500\pi, 4000\pi, 4500\pi, 5000\pi, 5500\pi]$ rad/s, while keeping the modulation amplitude constant *i.e.* $E_m = 42$ MPa. The results are provided in Figure 5(b), where, once again, the red lines represent the frequencies for which isolation and directional propagation of A0 mode can take place. It can be seen that the increase of ω_m leads to hardly any change in the width of the frequency band but raises the average frequency. This result suggests that there is a robust range of modulation frequency and propagation frequency for which mode isolation and unidirectional propagation of Lamb waves can be achieved.

As ω_m approaches 0, however, the frequency band for unidirectional wave travel to be viable would become vanishingly small [29] and therefore, the frequency bandwidth for mode isolation and non-reciprocal propagation would correspondingly decrease to 0 as well *i.e.* $\omega_m = 0$ is the lower bound for this phenomenon. As for the upper bound, ω_m should be sufficiently low so that the propagating wave can temporally resolve the oscillations of E and avoid unstable and time-growing modes. Its value is expected to be dependent on the material and modulation parameters and a derivation of its exact expression is non-trivial and will be investigated in future studies instead.

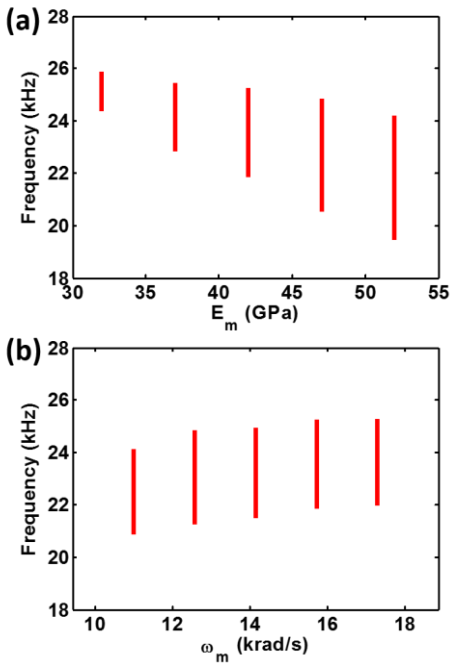

Figure 5: Range of propagating wave frequency where the S0 mode cannot propagate and the A0 mode can only travel unidirectionally in the -*x* direction, with respect to variations in the (a) amplitude of Young's modulus modulation, E_m and (b) angular frequency of modulation, ω_m.

3.4 Transmission analysis

Lastly, the transmission characteristics of individual Lamb wave mode in a spatiotemporally modulated thin plate was studied. To do this, two PZTs were attached at the top and bottom of the thin plate (Figure 6). When the voltages applied to the PZTs had a phase difference of zero, symmetric Lamb wave modes (S modes) were generated. When the applied voltages were out of phase by π radians, antisymmetric modes (A modes) will be generated.

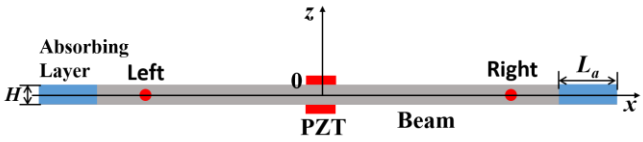

Figure 6: Two PZTs are used at the top and bottom of the plate to generate either symmetric or antisymmetric Lamb wave modes. Pure S0 Lamb wave mode can be generated by applying symmetric excitation signals onto

both PZTs, while A0 Lamb wave mode can be generated by applying asymmetric excitation signals.

The transmission coefficient (*TR*) of the Lamb wave displacement amplitude is defined as [44, 45]

$$TR = 20 \times \log(\frac{\mathcal{F}(ND)}{ref}) \quad (7)$$

where *ref* is a reference value, $\mathcal{F}$ indicates the Fourier transform and *ND*, the normalized displacement is expressed as

$$ND = \frac{sig}{sig_{ref}} \quad (8)$$

where *sig* is the displacement signal measured at a given position on the thin plate (red points in Figure 6) and sig_{ref} indicates the displacement signal measured at the excitation point on the plate (labelled '0' in Figure 6).

The transmission results are presented in Figure 7 for Constant Plate, Spatial Variation Plate and Spatiotemporal Variation Plate. In the results, *Left* indicates that the signal was measured at the location (*x*, *z*) = (-3, 0), while *Right* indicates that the signal was measured at the location (*x*, *z*) = (3, 0) (Figure 6). For Constant Plate, it can be seen from Figure 7(a) and (d) that *TR* for S0 and A0 are almost constant across the frequencies, which confirms that there is no bandgap for both Lamb wave modes. In addition, *TR (Left)* and *TR (Right)* are identical, indicating that there is no dependence on propagation direction. These results are consistent with the dispersion relation shown in Figure 3(b).

For the Spatial Variation Plate, it can be seen from Figure 7(b) and (e) that *TR* of both S0 and A0 were depressed at certain frequencies, which confirmed that there are bandgaps for both Lamb wave modes at *f* = 19.17 - 27.33 kHz for S0 mode and *f* = 20.04 – 22.38 kHz for A0 mode. This observation is consistent with the results in Figure 3(d). In addition. the *TR (Left)* and *TR (Right)* plots are essentially the same; the minute difference may have been due to slight variations in the mesh elements making up the left and right part of the plate. This result indicates that a spatially modulated plate can produce bandgaps while allowing for reciprocal propagation of waves.

For the Spatiotemporal Variation Plate, it can be seen from Figure 7(c) that the TR of S0 have some depressions, but they are slightly different for propagation to the *Left* (*f* = 18.15 – 25.73 kHz) and *Right* (*f* = 20.77 – 28.36 kHz) positions. In addition, it can be seen from Figure 7(f) that both *TR* (*Left*) and *TR* (*Right*) of A0 have depressions and they do not overlap. The bandgap for A0 is *f* = 17.42 – 19.75 kHz in the *-x* direction and *f* = 21.94 – 25 kHz in the *+x* direction, which suggests that the A0 mode can propagate unidirectionally in these frequency bands. This was confirmed above using an excitation signal with *f* = 24 kHz as an example.

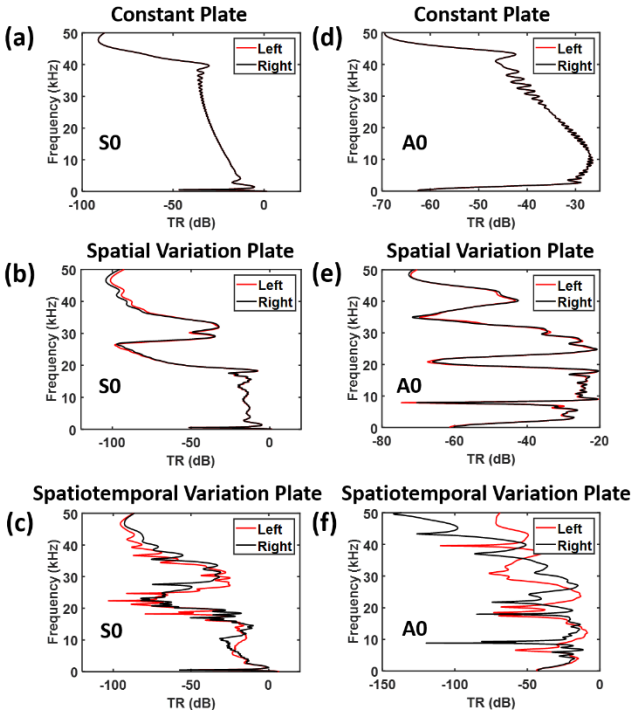

Figure 7 Transmission analysis for Constant Plate, Spatial Variation Plate and Spatiotemporal Variation Plate at different propagation frequencies. Plots of frequency against transmission coefficient (*TR*) of (a) S0 for Constant Plate, (b) S0 for Spatial Variation Plate, (c) S0 for Spatiotemporal Variation Plate, (d) A0 for Constant Plate, (e) A0 for Spatial Variation Plate, (f) A0 for Spatiotemporal Variation Plate.

3. Conclusions

In this report, we presented a numerical study investigating the asymmetric propagation of Lamb wave in a thin plate with periodic spatiotemporal variation of its Young's modulus. Fully coupled electro-mechanical finite element methods were developed to numerically simulate the propagation of Lamb waves in a uniform plate, a plate with spatial variation of Young's Modulus and a plate with spatiotemporal variation of Young's Modulus. The dispersion curve and transmission of

Lamb wave propagation were computed, and clearly showed that spatial variation of Young's modulus leads to the formation of bandgaps that can be used to isolate the Lamb wave modes, while the spatiotemporal variation of Young's modulus can lead to bandgaps and directional propagation, which can be used to isolate Lamb wave modes *and* reduce reflected waves in certain frequency ranges. In addition, it was ascertained that the frequency range for modal isolation and directional propagation can be tuned via the modulation parameters, such as the amplitude of Young's modulus modulation and modulation frequency. The insights derived in this study provide a design strategy to circumvent current limitations in Lamb-wave-based structure health monitoring and other potential applications, such as elastic mirrors, elastic sensors, filters and wave guides.

Acknowledgements

The authors would like to acknowledge funding for this project by the Temasek Research Fellowship.

Appendix

ANSYS software are used to model the coupling between PZT and the plate. The nodes between the PZT and the plate were connected, so that the bond between the plate and PZT was perfectly rigid. A potential difference was applied across the top and bottom planes of the PZT according to the excitation signal shown in Figure 2(a), in order to generate the symmetric and antisymmetric Lamb wave modes in the thin plate [46, 47]. The material properties of PZT are listed in Table 1 [48] and The PZT was modeled using the coupled field element (PLANE13) which links the mechanical and electrical degree of freedoms.

To solve this problem with good accuracy and high efficiency, a meshing strategy of appropriate mesh density had to be selected [49]. The maximum element size l_e and time step Δt to ensure accuracy was selected based on equation (6) and (7) [50]. In this study, we use $l_e = 5 \times 10^{-3}$ m and $\Delta t = 2 \times 10^{-6}$ s.

$$l_e = \frac{\lambda_{min}}{10} \quad (1)$$

$$\Delta t = \frac{1}{10 f_{max}} \quad (2)$$

where λ_{min} is the minimum wavelength and f_{max} is the maximum frequency studied.

Table 1: Material properties of PZT [48].

Young's Modulus (GPa)	
E_{11}	62
E_{33}	50
Poisson Ratio	0.3
Elastic Constant (GPa)	
C_{11}	110.8
C_{12}	49.8
C_{13}	49.8
C_{33}	110.8
C_{44}	30.5
Density (kg/m^3)	7800
Piezoelectric Constant (x 10^{-12} m/volt)	
D_{33}	650
D_{31}	-320
Coupling Coefficient	
k_{33}	0.75
k_{11}	0.44
Relative Dielectric Constant	
ε_{33}	3800

References

1. Filho, J.F.M.R., et al., *The feasibility of Structural Health Monitoring using the fundamental shear horizontal guided wave in a thin aluminum plate.* Materials, 2017. **10**(5): p. 551-560.
2. Giurgiutiu, V., *Tuned Lamb wave excitation and detection with piezoelectric wafer active sensors for structural health monitoring.* Journal of Intelligent Material Systems and Structures, 2005. **16**(4): p. 291-305.
3. Ong, W.H. and W.K. Chiu, *Designing for Lamb wave based in-situ structural health monitoring.* Key Engineering Materials, 2013. **558**: p. 411-23.
4. Santoni, G.B., et al., *Lamb wave-mode tuning of piezoelectric wafer active sensors for structural health monitoring.* Transactions of the ASME. Journal of Vibration and Acoustics, 2007. **129**(6): p. 752-62.
5. Park, I., Y. Jun, and U. Lee, *Lamb wave mode decomposition for structural health monitoring.* Wave Motion, 2014. **51**(2): p. 335-47.
6. Ostachowicz, W. and M. Radzienski. *Structural health monitoring by means of elastic wave propagation*. in *Modern Practice in Stress and Vibration Analysis 2012 (MPSVA 2012), 28-31 Aug. 2012*. 2012. UK: IOP Publishing Ltd.
7. Mitra, M. and S. Gopalakrishnan, *Guided wave based structural health monitoring: a review.* Smart

Materials and Structures, 2016. **25**(5): p. 053001 (27 pp.).
8. Schubert, K.J., C. Brauner, and A.S. Herrmann, *Non-damage-related influences on Lamb wave-based structural health monitoring of carbon fiber-reinforced plastic structures.* Structural Health Monitoring, 2014. **13**(2): p. 158-76.
9. Wu, T.-T., Wu, Z.-G. Huang, and S. Lin, *Surface and bulk acoustic waves in two-dimensional phononic crystal consisting of materials with general anisotropy.* Physical Review B (Condensed Matter), 2004. **69**(9): p. 94301-1.
10. Deymier, P.A., *Acoustic metamaterials and phononic crystals*. 2013, Berlin ; New York: New York : Springer.
11. Huang, G.L. and C.T. Sun, *Band Gaps in a Multiresonator Acoustic Metamaterial.* Journal of Vibration and Acoustics, 2010. **132**(3): p. 031003 (6 pp.).
12. Akozbek, N., et al., *Manipulating the extraordinary acoustic transmission through metamaterial-based acoustic band gap structures.* Applied Physics Letters, 2014. **104**(16).
13. Hou, Z. and B.M. Assouar, *Modeling of Lamb wave propagation in plate with two-dimensional phononic crystal layer coated on uniform substrate using plane-wave-expansion method.* Physics Letters A, 2008. **372**(12): p. 2091-7.
14. Zhao, M., et al., *Band gaps of Lamb waves propagating in one-dimensional periodic and nesting Fibonacci superlattices thin plates.* Thin Solid Films, 2013. **546**: p. 439-42.
15. Chen, J.-J. and X. Han, *The propagation of Lamb waves in one-dimensional phononic crystal plates bordered with symmetric uniform layers.* Physics Letters A, 2010. **374**(31-32): p. 3243-6.
16. Yao, Y., et al., *Thermal tuning of Lamb wave band structure in a two-dimensional phononic crystal plate.* Journal of Applied Physics, 2011. **110**(12): p. 123503 (4 pp.).
17. Zhu, X.-F., et al., *Investigation of a silicon-based one-dimensional phononic crystal plate via the super-cell plane wave expansion method.* Chinese Physics B, 2010. **19**(4): p. 044301 (6 pp.).
18. Chen, J.-J., F. Yan, and H.L.W. Chan, *Large Lamb wave band gap in phononic crystals thin plates.* Applied Physics B: Lasers and Optics, 2008. **90**(3-4): p. 557-559.
19. Hou, Z. and B.M. Assouar, *Numerical investigation of the propagation of elastic wave modes in a one-dimensional phononic crystal plate coated on a uniform substrate.* Journal of Physics D: Applied Physics, 2009. **42**(8): p. 085103 (7 pp.).
20. Sun, J.-H., et al. *A ZnO/silicon Lamb wave filter using phononic crystals*. in *2012 IEEE International Frequency Control Symposium (FCS), 21-24 May 2012*. 2012. Piscataway, NJ, USA: IEEE.
21. Serhane, R., et al., *Selective Band Gap to Suppress the Spurious Acoustic Mode in Film Bulk Acoustic Resonator Structures.* Journal of Vibration and Acoustics, 2018. **140**(3): p. 031018-031018-7.
22. Maznev, A.A., A.G. Every, and O.B. Wright, *Reciprocity in reflection and transmission: what is a 'phonon diode'?* Wave Motion, 2013. **50**(4): p. 776-84.
23. Chen, J.-j., X. Han, and G.-Y. Li, *Asymmetric Lamb wave propagation in phononic crystal slabs with graded grating.* Journal of Applied Physics, 2013. **113**(18): p. 184506 (6 pp.).
24. Li, J. and J.-j. Chen. *Unidirectional and tunable acoustic diode made by asymmetric double layer metallic grating with periodical structure*. in *2016 Symposium on Piezoelectricity, Acoustic Waves and Device Applications (SPAWDA), 21-24 Oct. 2016*. 2016. Piscataway, NJ, USA: IEEE.
25. Chaunsali, R., F. Li, and J. Yang, *Stress Wave Isolation by Purely Mechanical Topological Phononic Crystals.* Scientific Reports, 2016. **6**: p. 30662.
26. Wang, P., L. Lu, and K. Bertoldi, *Topological Phononic Crystals with One-Way Elastic Edge Waves.* Physical Review Letters, 2015. **115**(10): p. 104302.
27. Croenne, C., et al., *Brillouin scattering-like effect and non-reciprocal propagation of elastic waves due to spatio-temporal modulation of electrical boundary conditions in piezoelectric media.* Applied Physics Letters, 2017. **110**(6).
28. Swinteck, N., et al., *Bulk elastic waves with unidirectional backscattering-immune topological states in a time-dependent superlattice.* Journal of Applied Physics, 2015. **118**(6): p. 063103 (8 pp.).
29. Trainiti, G. and M. Ruzzene, *Non-reciprocal elastic wave propagation in spatiotemporal periodic structures.* New Journal of Physics, 2016. **18**(8): p. 083047 (22 pp.).
30. Attarzadeh, M.A. and M. Nouh, *Elastic wave propagation in moving phononic crystals and correlations with stationary spatiotemporally modulated systems.* AIP Advances, 2018. **8**(10): p. 105302.
31. Ansari, M.H., et al., *Application of magnetoelastic materials in spatiotemporally modulated phononic crystals for nonreciprocal wave propagation.* Smart Materials and Structures, 2018. **27**(1): p. 015030.
32. Popa, B.I., Y. Zhai, and H. Kwon, *Acoustic bianisotropic metasurfaces for broadband non-reciprocal sound transport.* The Journal of the Acoustical Society of America, 2018. **144**(3): p. 1831-1831.
33. Attarzadeh, M.A., H. Al Ba'ba'a, and M. Nouh, *On the wave dispersion and non-reciprocal power flow in space-time traveling acoustic metamaterials.* Applied Acoustics, 2018. **133**: p. 210-214.

34. Attarzadeh, M.A. and M. Nouh, *Non-reciprocal elastic wave propagation in 2D phononic membranes with spatiotemporally varying material properties.* Journal of Sound and Vibration, 2018. **422**: p. 264-277.
35. Arkadii Krokhin, A.N., Ezekiel Walker,Andrey Bozhko, *Non-reciprocal acoustic transmission through a dissipative phononic crystal with asymmetric scatterers (Conference Presentation.* Proc.SPIE, 2018. **10600**.
36. Zanjani, M.B., et al., *One-way phonon isolation in acoustic waveguides.* Applied Physics Letters, 2014. **104**(8): p. 081905.
37. Wang, Y., et al., *Observation of nonreciprocal wave propagation in a dynamic phononic lattice.* Physical Review Letters, 2018.
38. Naizhi, Z. and Y. Shi. *Experimental research on damage detection of large thin aluminum plate based on Lamb wave*. in *Sensors and Smart Structures Technologies for Civil, Mechanical, and Aerospace Systems 2010, 8-11 March 2010*. 2010. USA: SPIE - The International Society for Optical Engineering.
39. Giurgiutiu, V., *Structural health monitoring with piezoelectric wafer active sensors*. 2008, Amsterdam ; Boston: Academic Press.
40. *ANSYS 15.0, Help Electromagnetic analysis guide.*
41. Semblat, J.F., L. Lenti, and A. Gandomzadeh, *A simple multi-directional absorbing layer method to simulate elastic wave propagation in unbounded domains.* International Journal for Numerical Methods in Engineering, 2011. **85**(12): p. 1543-63.
42. Kwok, K.W., et al. *Self-polarization in PZT films*. 2002. Taylor and Francis Inc.
43. Ruzzene, F.R.a.M., *Wave propagation in linear and nonlinear periodic media : Analysis and applications*. 2012, New York: Springer.
44. Van Belle, L., et al. *Sound transmission loss of a locally resonant metamaterial using the hybrid wave based - finite element unit cell method*. in *2017 11th International Congress on Engineered Materials Platforms for Novel Wave Phenomena (Metamaterials), 27 Aug.-2 Sept. 2017*. 2017. Piscataway, NJ, USA: IEEE.
45. Ang, L.Y.L., Y.K. Koh, and H.P. Lee, *Plate-type acoustic metamaterial with cavities coupled via an orifice for enhanced sound transmission loss.* Applied Physics Letters, 2018. **112**(5): p. 051903 (5 pp.).
46. Liu, W. and V. Giurgiutiu. *Finite element simulation of piezoelectric wafer active sensors for structural health monitoring with coupled-filed elements*. in *Sensors and Smart Structures Technologies for Civil, Mechanical, and Aerospace Systems 2007, 19 March 2007*. 2007. USA: SPIE - The International Society for Optical Engineering.
47. Yang, J., *Special Topics in the Theory of Piezoelectricity*. 2009, New York: Springer.
48. Song, F., et al., *On the study of surface wave propagation in concrete structures using a piezoelectric actuator/sensor system.* Smart Materials and Structures, 2008. **17**(5): p. 055024 (8 pp.).
49. Zhao, L., S.C. Conlon, and F. Semperlotti, *Broadband energy harvesting using acoustic black hole structural tailoring.* Smart Materials and Structures, 2014. **23**(6): p. 065021 (9 pp.).
50. Shen, Y. and V. Giurgiutiu, *Predictive modeling of nonlinear wave propagation for structural health monitoring with piezoelectric wafer active sensors.* Journal of Intelligent Material Systems and Structures, 2014. **25**(4): p. 506-520.